# DESIGN AND SIMULATION OF SOLAR PHOTO VOLTAIC BASED ANION EXCHANGE MEMBRANE ELECTROLYZER FOR HYDROZEN PRODUCTION

Kota.Vardhan
*dept. of Electrical and Electronics Engineering*
*Aditya Institute Of Technology And Management Tekkali,Srikakukalm,A.p-532201*
Tekkali, India

Pondara.Lokesh
*dept. of Electrical and Electronics Engineering*
*Aditya Institute Of Technology And Management Tekkali,Srikakukalm,A.p-532201*
Tekkali, India

Kanthumahanti.Sriya
*dept. of Electrical and Electronics Engineering*
*Aditya Institute Of Technology And Management Tekkali,Srikakukalm,A.p-532201*
Tekkali, India

Sana.Devika
*dept. of Electrical and Electronics Engineering*
*Aditya Institute Of Technology And Management Tekkali,Srikakukalm,A.p-532201*
Tekkali, India

Bala Murali. Pydi
*dept. of Electrical and Electronics Engineering*
*Aditya Institute Of Technology And Management Tekkali,Srikakukalm,A.p-532201*
Tekkali, India

Corresponding Author : Bala Murali. Pydi

***Abstract:*** **Anion exchange membrane (AEM) water electrolysis is a new technique that can fill the gap between traditional alkaline electrolysis and expensive proton exchange membrane (PEM) systems. This through analysis covers operating parameters, membrane – electrode assembly (MEA) fabrication techniques, necessary materials (membranes, catalysts, ionomers), and system -level Integration in order to summarise current advancements in AEM water electrolysis. The technique combines the economic advantage of alkaline electrolysis, such as the use of platinum -group -metal- free (PGM- free) Catalysts and stainless -steel bipolar plates, with the compactness, dynamic responsiveness, and pure water operation of PEM systems. However, there are still a lot of un answered questions. The primary obstacles to industrial commercialization are membrane breakdown mechanisms, limited long- term durability (now usually below 2000 h in laboratory experiments), and inadequate chemical stability in alkaline settings. This review indicates the activation polarization dominates cell voltage losses, membrane ionic conductivity and stability need to be significantly enhanced, and systematic integration methods with intermittent renewable energy resources are currently lacking. This work includes a literature reviews as well as MATLAB /Simulink – based system- level model of an AEM electrolyser connected to renewable energy sources. To optimize power transfer and operating conditions at the electrolyser terminals, a DC-DC buck converter and maximum power point tracking (MPPT) techniques are used. We suggest a research roadmap towards technology readiness level (TRL) 4-5 systems appropriate for pilot-scale deployment, based on significant discoveries from scholarly studies published between 2012 and 2025 and recent commercial demonstrations. For successful large-scale commercialization of AEM water electrolysers, the study emphasizes the necessity of coordinated development of chemically stable membranes with ionic conductivity ≥ 100 mS/cm under Operating conditions, robust PGM- free catalyst systems, a mechanistic understanding of degradation pathways, and validated dynamic control strategies, such as MPPT- based power conditioning via DC-DC converters.**

***Keywords:*** ***Anion exchange membrane, water electrolysis, green hydrogen, alkaline electrolyser, membrane materials, electro catalysts, PGM – free catalysts, electrochemical degradation, renewable energy integration, hydrogen Production.***

## *I. INTRODUCTION*

With current global production surpassing 100 million tonnes annually, hydrogen has emerged as a crucial energy carrier in the global shift towards sustainable

and low -carbon energy systems [1]. However, fossil fuel- based techniques like steam methane reforming now create over 99% of hydrogen, which results in substantial carbon dioxide emissions of about 9-12 tonnes $CO_2$ per tonne of hydrogen [2]. This has increased the demand for sustainable and clean methods of producing hydrogen, especially those they rely on water electrolysis powered by renewable energy [3]. Alkaline water electrolysis (AWE), which offers lengthy operational lifetimes surpassing 60,000 hours and large-scale industrial deployment, is the most developed and extensively used electrolysis technology currently available [4]. Despite its maturity, AWE has a number of drawbacks, such as limited part-load operation, delayed dynamic response, and safety issues because of gas crossing at low current densities [5], [6], [7]. Furthermore, the need for concentrated alkaline electrolytes raises system complexity and presents problems with material corrosion [8]. Because of its small size, high current density operation, and quick dynamic reaction, proton exchange membrane (PEM) electrolysis has drawn interest and can be integrated with intermittent renewable energy sources [9],[10],[11]. However, PEM systems economic scalability is limited by their heavy reliance on costly corrosion- resistant components and noble metal catalysts like platinum, iridium, and ruthenium [12], [13]. Anion exchange membrane (AEM) water electrolysis, which combines the benefits of both alkaline and PEM systems, has become a viable solution to these problems [14]. Non-precious metal catalysts like nickel, iron, and cobalt can be used in AEM electrolyzers because they use solid polymer membranes that transport hydroxide ions($OH^-$) in an alkaline environment [15], [16]. Compared to traditional alkaline systems this greatly lowers material costs while preserving better gas separation and operating flexibility[17], [18]. Despite these benefits, AEM technology is still in its infancy, and a number of obstacles prevent widespread commercialization. These include problem with catalyst – membrane integration, poor ionic conductivity in comparison to PEM systems, membrane degradation in alkaline settings, and a lack of long term durability data [19], [20], [21], [22]. Additionally, not enough research has been done on system level integration with renewable energy sources, especially in dynamic operating environments [23]. Sustainable hydrogen production is made possible by combining electrolyzers with renewable energy sources, particularly solar photovoltaic (PV) systems [24]. Electrolysers electrolysers can directly use the direct current (DC) energy produced by solar photovoltaic systems; however, The inherent unpredictability in solar irradiation causes fluctuating power output, which impacts electrolyser performance and hydrogen production efficiency [25],[26]. Therefore to optimize hydrogen yield, effective power management techniques are crucial. In order to harvest maximum power from PV systems under a variety of environmental situations, maximum power point tracking (MPPT) approaches are essential [27]. The perturb and observe (P&O) algorithm is one of the most popular MPPT techniques because of its simplicity and ease of use [28], [29]. MPPT guarantees the best possible energy transfer to the electrolyser by continuously modifying the PV systems operating point. Additionally, DC-DC converters, especially buck converters are frequently used to control the voltage and current levels between the electrolyser and the PV systems [30]. By aligning the PV panels operational parameters with the electrolyser's specifications, these converters enhance the system's overall stability and efficiency [31]. Although direct coupling of PV systems to electrolysers provides a straight forward and in expensive design, the mismatch between PV output characteristics and electrolyser load requirements frequently leads to unsatisfactory performance [32]. On the other hand, better use of available solar energy is made possible by combining MPPT management with power electronics converters, which results in increased hydrogen generation [33], [34]. The significance of dynamic electrolyser functioning under renewable energy inputs has been emphasizes by recent research, under scoring the necessity of advanced control strategies and systems optimization [35],[36]. Compared to conventional alkaline systems, AEM electrolyzers are especially well-suited for such applications due to their quick response time and adaptable working range [37]. MATLAB/SIMULINK and other modeling and simulation tools offer an efficient platform for analysing system performance, optimizing design parameters, and assessing various control techniques under various operating situations [38],[39]. Without the need of costly experimental equipment, simulation

-based research allow for a thorough examination of system behaviour. Thus, the modeling and comparative analysis of hydrogen generation utilising an AEM electrolyser powered by a solar PV systems is the main emphasis of this study. Two configurations are examined: (1) the PV panel is directly coupled to the AEM electrolyser, and (2) MPPT is integrated utilising a DC-DC buck converter and the perturb and observe algorithm. MATLAB/Simulink is used in the development and analytics of the entire system to assess performance in terms of power consumption, system stability, and hydrogen generation efficiency.

## *II. CONTROLLING TOPOLOGY*

### *1. Controlling of solar PV Array*

A solar photovoltaic (PV) array is a configuration of solar panels connected to generate electricity of solar panels connected to generate electricity from sunlight. It is main source of power in a solar power system. When several solar panels are connected in series and parallel, a solar PV array is produced. Numerous sun cells makeup each solar panel. The array increases its power output to meet the required electrical load. A solar PV array's operation is based on the photovoltaic effect. When sunlight strikes solar cells, the semiconductor material-typically silicon- absorbs photons and releases electrons. As these electrons move across the external circuit, electric current is produced. For use in homes and businesses, direct current (DC) power is converted into alternating current (AC) using an inverter.

A solar PV array is made up of a number of essential parts. These include solar cells and solar modules (panels), cables, connectors, junction boxes, DC combiner boxes, and mounting structures. The panels are supported by a mounting mechanism at a fixed tilt angle to optimize sunlight. The combiner box collects power from multiple strings while guarding against over currents and lightning surges. A solar PV array's panels can be connected in series or parallel. A series connection raises the output voltage, while a parallel connection raises the output current. By establishing the proper configuration, the array output is matched with the inverter and load requirements. There are several types of solar PV arrays, including as grid-connected, off-grid and hybrid. Grid connected arrays are linked to the utility grid and have the ability to export excess power. In remote areas, off-grid arrays with battery storage are utilised. Hybrid systems combine battery and grid technology to offer a stable power supply. There are several benefits to solar photovoltaic arrays. They provide clean, renewable energy, have a long lifespan of about 25 to 30 years, reduce electricity costs, and need little upkeep. They are widely used in water pumps, solar power plants, homes, telecom towers, and street lighting systems.

### *2. Sun tracking mechanism*

A sun tracking mechanism is a system that constantly rotates solar panels to face the sun directly. This increases the amount of solar energy captured as compared to stationary solar panels. A duel axis sun tracker can follow the sun both vertically and horizontally throughout the day and in all seasons since it's solar panel can move in two different directions. The dual axis sun tracker works by tracking the sun's path across the sky. The sun moves from east to west throughout the day, and it's altitude in the sky varies with the seasons. The tracker uses two rotational axis: the elevation axis, which moves vertically, and the azimuth axis, which moves horizontally.

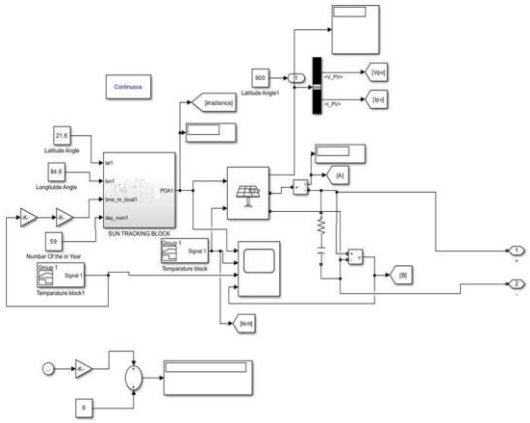


*Fig 1 : Controlling Diagram of sun tracking block*

Different parts make up a dual-axis tracking system. Motor drivers, DC or stepper motors, sensors (such light or LDR sensors), a microcontroller (like an Arduino or PLC), and a mechanical framework to secure the panel are the components of these systems. When the sensors detect the direction of the strongest sunlight, they alert the controller. The controller reads the signals and drives the motors to spin the panel in the desired direction. Dual axis trackers can operate in two different ways: sensor-based and time-based. In sensor-based systems, light sensors continuously gauge the amount of sunlight and adjust the panel position. Using pre-programmed sun position data

based on the place and time, the controller in time-based systems rotates the panel. Advanced systems use GPS and astronomical algorithms for accurate tracking.

### 3. DC-DC converter

Power is effectively transferred from a lower DC input voltage to a higher DC output voltage using a power electronics circuit called a DC-DC boost converter or setup converter. When the voltage supplied by the available power source – such as a battery, solar cell, or fuel cell-is insufficient to match the demands of the load, it is commonly used in electronic systems. The boost converter uses high- frequency switching and energy storage components to enhance the voltage without the need for transformers, making it lightweight, compact, and suitable for modern electronic equipment.

The basic parts of a boost converter are an output capacitor, control circuit, diode (or synchronous switch), inductor, and controlled switch (often a MOSFET). These components store the energy from the input source and release it at a grater voltage. The control circuit controls the switching operation to ensure that the output voltage stays constant despite variations in the input voltage or load conditions. To comprehend how a boost converter works, one might look at its two main switching states. When the switch is activated, the input voltage is applied across the inductor, increasing the inductor current and storing energy in its magnetic field. The diode reverse biasing isolated the output from the input during this period, and the load is powered by the energy stored in the output capacitor. We refer to this phase as the energy storage phase.

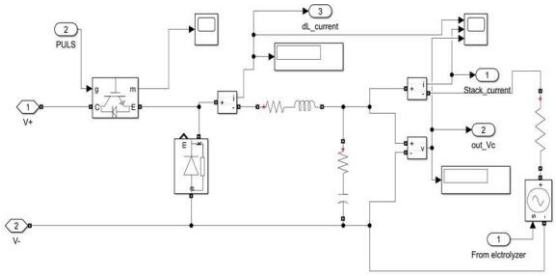


*Fig 2 : Controlling Diagram of DC-DC buck converter*

When the switch is switched off, the inductor tries to keep the current flowing, which reverse the voltage's polarity. The energy stored in the inductor is transferred to the output capacitor and load by raising the input voltage and forward-biasing the diode. As a result, the output voltage was higher than the input voltage. By repeating this procedure at a high frequency, the converter can raise the voltage continually.

### 4. MPPT controller

Solar power systems use an MPPT controller, an advanced kind of charge controller, to maximise the electricity produced from solar panels. MPPT stands for Maximum Power Point Tracking. The temperature and amount of sunlight effect the voltage and current that solar panels produce. To optimum power extraction, the MPPT controller adjusts the operating point while continuously monitoring the solar panel's maximum power point. An MPPT controller operates based on the V-I and P-V characteristics of a solar panel. Every solar panel has a maximum power output at a specific voltage and current. This posture is known as the maximum power position(MPP). The MPPT controller uses algorithms like Hill climbing, Incremental Conductance, Perturb and Observe (P&O) to find this point and keep the panel operating even when external conditions change.

An MPPT controller is mostly composed of a microprocessor, sensors, control, and DC-DC converter of the buck, boost, or buck-boost type adjusts the voltage and current of the solar panel to suit the requirements of the battery or load. The computer determines the power, measures the panel voltage and current, and controls converter switching to maintain the converter running at its maximum power point.

### 5. MPPT techniques

Maximum power point Tracking (MPPT) control methods are used by solar photovoltaic (PV) systems to optimise the amount of electricity that solar panels can generate. The quantity of sunlight, temperature, and shade all affect the voltage and current that solar panel's produce. By continuously adjusting the solar panel's operating point (MPP), MPPT techniques boost the efficiency of the solar power system.

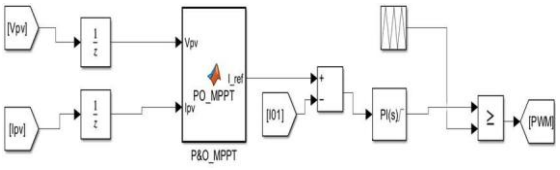


*Fig 3 : Controlling diagram of P&O MPPT technique*

*Perturb and Observe (P&O) MPPT technique*

One of the most popular MPPT algorithms for solar PV systems is Perturb and Observe(P&O), sometimes referred to as the hill-climbing method. Its primary objective is to maintain the PV panel's maximum power point where the voltage and current product is highest despite the fact that temperature and irradiance constantly alter the panel's characteristics. The program observes the change in output power that occurs when the PV voltage or the DC-DC converter's duty cycle is slightly altered. The controller drives the operating point toward and maintains it close to the maximum power point if the power increases after the disturbance; if the power lowers, it reverse the direction. In a real-world application, a microcontroller or DSP measures the PV voltage and current, calculates the instantaneous power, compares it to the prior value, and modifies the converter duty cycle as necessary. P&O is widely used in commercial MPPT charge controllers and small and medium sized PV systems due to its simplicity, affordability, and ease of implementation. Although its durability and simple complexity make it one of the most often used MPPT algorithms in practice, it can mis-track or respond slowly when irradiance changes quickly, and it naturally produces little oscillations around the MPP that result in slight power losses.

## III. DYNAMIC MODELLING OF AEM WATER ELECTROLYSER

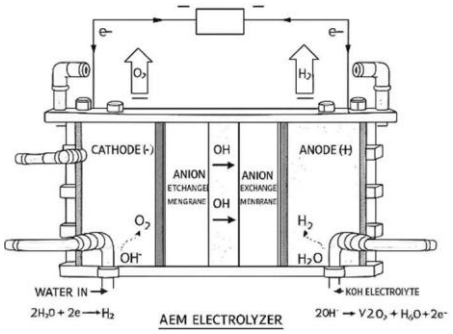


*Fig 4 : Schematic diagram of single cell of AEMWE*

### *1. AEM electrolyzer polarization curve*

The electrochemical reactions response time is acknowledged as being quite quick in comparison to other physical processes occurring inside the AWE system. Therefore, it can be said that a static approach is adequate to forecast the system characteristics in a simulation at the system level [40].

The net voltage is calculated by adding the reversible, activation, and ohmic over voltages.

$$V_{cell} = E_{rev} + V_{act-c-\theta} + V_{act-a-\theta} + V_{ohm} \quad (1)$$

### *2. Reversible voltage*

$V_{ohm}$ stands for ohmic voltage, $E_{rev}$ for reversible voltage, and $V_{act-c-\theta}$ and $V_{act-a-\theta}$ for cathode and anode activation voltage, respectively. Diffusion over voltage has a greater impact on the cell when operating at a high current density. It is not considered since it has minimal impact on alkaline water electrolysis, which operates at a comparatively low current density. The reversible voltage is computed using the Nernst equation.

$$E_{rev} = E^{*}_{rev} + \frac{RT}{2F} \ln\left(\frac{(P - P_{H2O})^{1.5} \; P^{*}_{H2O}}{P_{H2O}}\right) \quad (2)$$

Where $E_{rev}$ is the standard potential and P, T, R, and F are the operating pressure, temperature, constant, and universal gas constant. $P_{H2O}$ is the pressure of the humid hydrogen and oxygen and oxygen gases at the electrode, and $P^{*}_{H2O}$ is the vapour pressure of pure water. The first term, which represents the standard potential, is very temperature dependent and can computed as follows [41]:

$$E_{rev}(T) = 1.50342 - 9.956 \times 10^{-4} T + 2.5 \times 10^{-7} T \quad (3)$$

The second term represents the effect of pressure on the reversible potential. The correlations proposed by Leroy [42] are used to derive both $P_{H20}$ and $P^{*}_{H20}$. The influence of temperature-dependent molarity in $P\_H_2O$ can be expressed using the temperature and weight percent (wt%) of the KOH solution [41]:

$$P^{*}_{H20} = T^{-3.4159} \exp\left(37.043 - \frac{6275.7}{T}\right) \quad (4)$$

$$P_{H20} = T^{-3.4159} \exp\left(37.043 - \frac{6275.7}{T}\right) x \exp\left(0.016214 - 0.13082m + 0.1933m^{0.5}\right) \quad (5)$$

$$m = w \frac{(183.1221 - 0.5684 + 984.5679 \exp(\frac{w}{115.96277}))}{5610.5} \quad (6)$$

The activation over voltage is the potential difference that is applied when an electrochemical reaction moves out of equilibrium and begins to flow ahead. It takes place at both electrodes and the over voltage on the anode side appears to be higher in the majority of situations. The Butler-volmer formula was typically used to determine the activation's over voltage [41].

$$V_{act} = \frac{RT}{F\alpha_a} \sinh^{-1}\left(\frac{j}{j_{0,a}}\right) + \frac{RT}{F\alpha_c} \sinh^{-1}\left(\frac{j}{j_{0,c}}\right) \quad (7)$$

Where $j\_(0,a)$ and $j\_(0,c)$ are the exchange current densities and $\alpha_a$ and $\alpha_c$ are the charge transfer

coefficients for anode and cathode processes, respectively.

The forward and backward reactions that take place at the anode and cathode surfaces in this model have the same charge transfer coefficient. The exchange current density coefficients of the Ni electrodes used for the anode and cathode can be calculated as follows using the data in Ref [43].

$$j_{0,a} = 1.5 \times 10^{-4} \left(\frac{P}{P_{ref}}\right)^{0.1} \exp\left[-\frac{23000}{RT}\left(1 - \frac{T}{T_{ref}}\right)\right] \quad (8)$$

$$j_{0,c} = 0.9 \times 10^{-4} \left(\frac{P}{P_{ref}}\right)^{0.1} \exp\left[-\frac{42000}{RT}\left(1 - \frac{T}{T_{ref}}\right)\right] \quad (9)$$

The formula derived from the experimental data is used to determine the charge transfer coefficient [43].

$\alpha_a = 0.07835 + 0.001T$ (10)

$\alpha_c = 0.1175 + 0.00095T$ (11)

### 3. Ohmic Over Potential

The transport of an electron or ion results in an ohmic over voltage. The primary components of the electrolysis cell are the electrodes, electrolyte, and membrane; the opposition of the bipolar plates is believed to be negligible. According to ohm's law, the overvoltage can be calculated can be calculated by multiplying the total resistance and current.

$V_{ohm} = I(R_{Cathode} + R_{Anode} + R_{K0H} + R_{mem})$ (12) The electrode resistance and resistance and electrolyte resistance are computed as follows using the conductivity of the anode and cathode sides:

$$R = \frac{1}{\sigma}\left(\frac{L}{S}\right) \quad (13)$$

Where L and S represent the electrode's active area and thickness, respectively. The electrical conductivity($\sigma_{Ni}$) of the Ni electrodes is determined using the correlation as a function of temperature:

$$\sigma_a = \sigma_c = \sigma_{Ni} = 60000000 - 279650T + 532T^2 - 0.380577T^3 \quad (14)$$

Gilliam and associates this link indicates that electrical conductivity, which peaks at roughly 30 weight percent, is influenced by temperature and molar concentration [44].

$$\sigma_{K0H} = -2.041m - 0.0028m^2 + 0.005332mT + 207.2\frac{m}{T} + 0.001043m^3 - 0.0000003T^2m^2 \quad (15)$$

The following formula can be used to calculate the resistance for the 0.5 mm-thick Zircon membrane in the 30 weight percent KOH electrolyte [43]:

$$R_{mem} = \frac{0.06 + 80e^{-\frac{T}{50}}}{10000S_m} \quad (16)$$

The bubbles created by the oxygen and hydrogen gases have two effects on AWE's performance. These bubbles first cover the electrode surface, decreasing the electrode's active area. As the active region shrinks, the activation overvoltage increases. Second, the bubbles lower the electrolyte's electrical conductivity as they move across it, which eventually causes the ohmic overvoltage to increase. The electrode area covered by bubbles can be calculated using a ratio known as the covering coefficient or $\theta$.

$$S_{available} = S_{total}(1 - \theta) \quad (17)$$

Since it is believed that the bubbles are spherically formed and that the electrode is covered by their cross-sectional area, the change in active area is proportionate to the rise in temperature and fall in pressure. The covering coefficient correlation, which is a unique function of current density, can therefore be used to account for both the pressure and temperature contributions by combining the bubble volume fluctuation with the temperature and pressure changes.

$$\theta = 0.023(j)^{0.3}\left(\frac{T}{T_{ref}}\frac{P_{ref}}{P}\right)^{\frac{2}{3}} \quad (18)$$

As a result, the activation overvoltage, which accounts for the bubble's impact could be determined as follows:

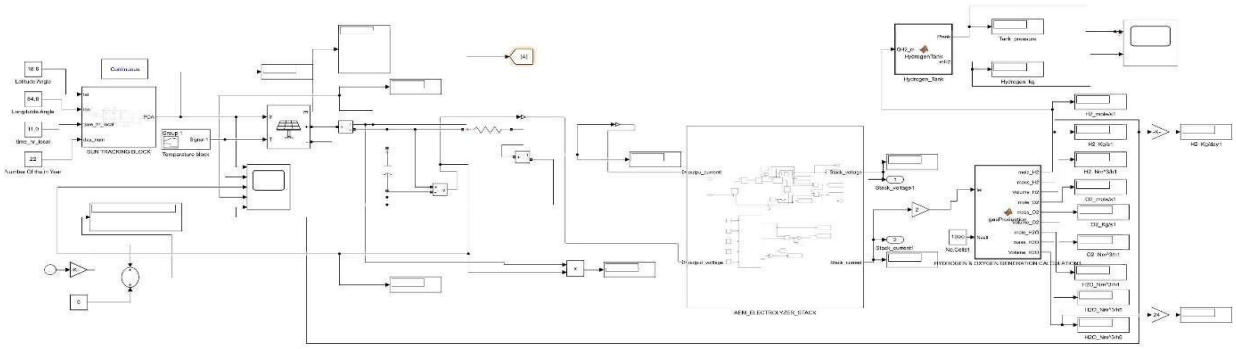

*Fig: Schematic block diagram for simulation of proposed work*

*4. Activation over potential*

$$V_{act-} = \frac{RT}{F\alpha_a} \sinh^{-1}\left(\frac{1}{S(1-\theta)}\right) + \frac{RT}{F\alpha_c} \sinh^{-1}\left(\frac{S(1-\theta)}{j_{0,c}}\right) \quad (19)$$

The equation can also be written as follows:

$$V_{act-\theta} = \left[\frac{RT}{F\alpha_a} \sinh^{-1}\left(\frac{j}{j_{0,a}}\right) - \frac{RT}{F\alpha_a} \sinh^{-1}(1-\theta)\right] + \left[\frac{RT}{F\alpha_c} \sinh^{-1}\left(\frac{j}{j_{0,c}}\right) - \frac{RT}{F\alpha_a} \sinh^{-1}(1-\theta)\right] \quad (20)$$

*5. Bruggeman Equation*

The second effect-the electrolytes decreased electrical conductivity as a result of the "bubble effect" –can be calculated using the Bruggeman equation [45]. The percentage of bubbles that effect the original and current conductivity is stated as a function of ε, which can be obtained in proportion to θ.

$$\frac{\sigma_{K0H-bubble}}{\sigma_{K0H}} = (1-s)^{\frac{2}{3}} \quad (21)$$

$$s = \frac{2}{3}\theta \quad (22)$$

Therefore, the electrolyte resistance is calculated as follows while taking the bubble effect into account:

$$R_{K0H-bubbl} = \frac{1}{\sigma_{K0H}(1-s)^{1.5}}\left(\frac{d_{am}}{S_a} + \frac{d_{cm}}{S_c}\right) \quad (23)$$

*6. Flow of gases products and water costumed*

The production rate of hydrogen determined as follows:

$$n_{H_2,prod} = 5 \; F \frac{iA}{2F} n_{cell} \quad (24)$$

The faraday efficiency, or η_F, is the ratio of the hydrogen generation rate to the supplied current. This study assumes that η_F=1 by ignoring hydrogen losses such as diffusion over the diaphragm. Additionally, the reaction formula can be used to ascertain how oxygen and water react:

$$n_{H_2O} = n_{H_2,prod} \quad (25)$$

$$n_{O_2,prod} = \frac{1}{2} n_{H_2,prod} \quad (26)$$

When the voltage in the AWE stack rises above the thermos neutral voltage, heat is produced. The amount of power required to create the heat for reasonable temperatures of the reactant and product, as well as the production of hydrogen, can be used to calculate the quantity of heat produced:

$$Q_{excess} = H_{ca-inlet} + W_{stack} - H_{ca-outlet} - H_{an-outle} \quad (26)$$

Where $W_{stack}$, which is determined by the applied voltage and current, is the electric power input for the electrolysis process.

$$W_{stack} = V_{cell}(j \times A) n_{cell} \quad (27)$$

## IV. Simulation & Results

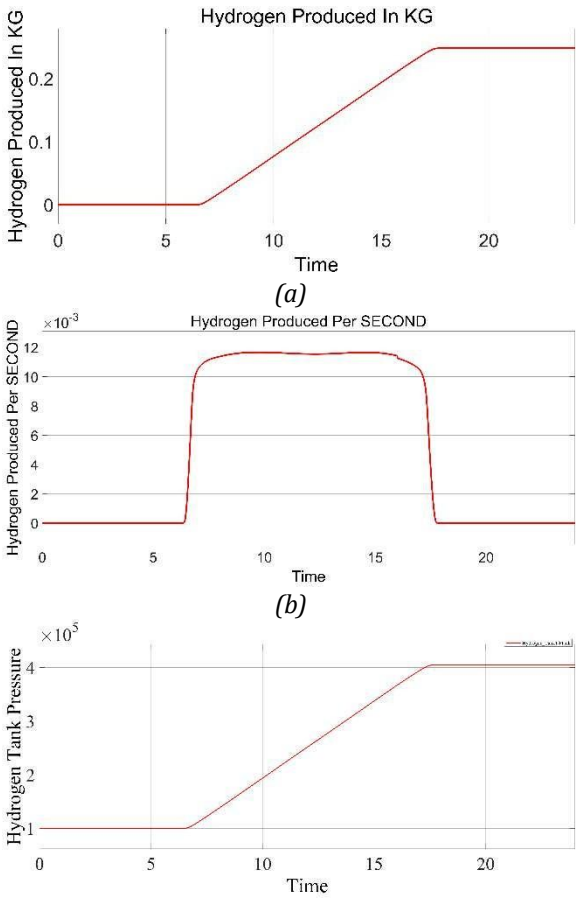


*Fig 4(a) Hydrogen Produced In Kg , 4(b)Hydrogen Per Sec , 4(c) Hydrogen Tank Pressure with MPPT.*

The "hydrogen produced in kg" graphic illustrates this as a smooth, nearly linear rise from around 7:00 to approximately 18:00. When the sun sets and production ceases, the curve flattens, resulting in a final daily output for this simulated scenario of about 0.25 kilogram. The tank-pressure plot confirms that MPPT-controlled operation charges the storage vessel effectively and without significant transients: pressure remains close to its initial value early in the morning, then rises almost linearly as hydrogen builds up in the tank, finally saturating at a nearly constant maximum once production stops in the evening.

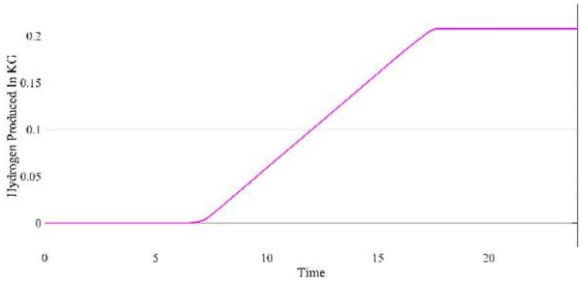


*(d)*

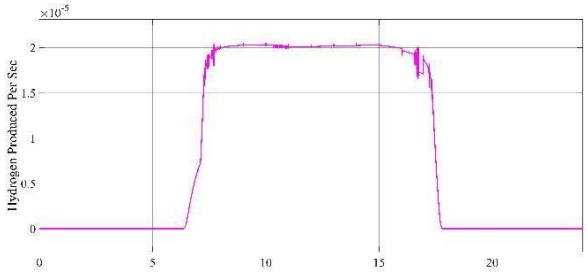


*(e)*

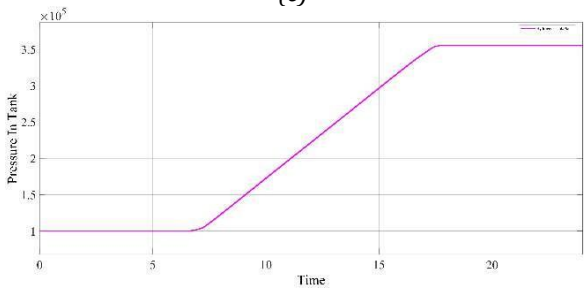


*(f)*

*Fig 4(d) Hydrogen Produced In Kg , 4(e)Hydrogen Per Sec , 4 (f) Hydrogen Tank Pressure without MPPT.*

The outcomes show how the system's hydrogen generation and storage operate dynamically. At first, the hydrogen output is 0 kg, indicating no electrolysis, and the hydrogen tank pressure stays constant at about $1 \times 10^1$ Pa. The production of hydrogen starts after around six seconds, resulting in a linear increase in both values. The generation of hydrogen reaches around 0.21 kg as the tank pressure gradually rises to about $4.05 \times 10^1$ Pa. Controlled hydrogen inflow is indicated by the short-time pressure graph's tiny step increases from $2.510 \times 10^1$ Pa to $2.523 \times 10^1$ Pa. A steady output rate under stable operational circumstances is shown by the linear trend. Pressure and hydrogen production eventually stabilise, indicating that either the system shuts down for safety or the storage limit is achieved, guaranteeing effective and controlled functioning.

Under reference circumstances, a large alkaline water electrolyser stack with 1,090 cells of 729 $cm^2$ each, operating with 30 weight percent KOH at a current density of 0.6 $A/cm^2$ and roughly 70 ºC, produces about 200 $NM^3/h$ of hydrogen at near-atmospheric pressure. In -depth numerical modelling of a pressurised AWE system at this operating point yields stack power of about 888 kW and total system power of about 918 kW at 1 bar, which translates to a system efficiency of about 76.9% on a higher heating value (HHV) basis. The same study demonstrates that system efficiency first rises(79.1% at 10 bar) when stack pressure grows from 1 to100 bar at fixed current density and hydrogen generation, and then marginally declines as more pressurisation losses take over (78.1% at 100bar).

Due to the significant decrease in residual water vapour content at greater pressure, the modelled AWE system improves hydrogen purity from about 97.3% at 1 bar to 99.6% at 5 bar and roughly 99.98% at 100 bar at condenser temperatures of around 20 ºC and stack temperature of 70 ºC. because smaller gas bubbles lower electrolyte and electrode resistances, the reversible cell voltage rises from roughly 1.178 V to 1.285 V over the same pressure range, while activation and ohmic over voltages fall. As a result, the necessary cell voltage only slightly varies between 1 to 100 bar at a given current density.

The AWE stack and balance-of-plant (BOP) for the current solar-powered system are considered to be same as those in the cited model, with the same number of cells, active area, electrolyte concentration, temperatures, and hydrogen production objective of 200 $Nm^3/h$ at 0.6 $A/cm^2$. In order to replicate the 200 $Nm^3/h$ reference operating point in the “with MPPT” scenario, the solar PV field, MPPT controller, and DC-DC buck converter are sized so that, under design irradiance, the DC power available at the electrolyser DC bus is sufficient to supply the nominal stack power (≈888 kW) plus BOP electrical demand (primarily compressor and fans). A 20% decrease in useful DC power transferred from the PV array (for instance, when operating without MPPT and buck converter) is assumed to result in an approximate 20% drop in the steady-state hydrogen production rate at similar cell voltage and temperature because electrolyser hydrogen production is directly proportional to the DC current passed through the stack at fixed operating voltage.

For the solar-coupled simulations, a representative stack pressure of 10 bar is chosen for compactness and in accordance with published efficiency trends because this pressure is close to the reported optimal region (10-30 bar) where overall system efficiency, including compression to higher delivery pressure, is assumed to operate at 20 ºC, which is sufficient to

achieve hydrogen purity is slightly lower but still above 99.5%, consistent with typical industrial alkaline electrolysers without additional dryers.

A consistent set of single-page simulation results for the solar-driven AWE system is summarised in table1. The "with MPPT + buck" case shows the 20% decrease in hydrogen production seen experimentally in the user's project.

The stack can operate at the design current density of 0.6 A/cm$^2$ and produce the reference 200 Nm$^3$/h of hydrogen at about 10 bar with high system efficiency and >99.5% purity in the with-MPPT scenario because the PV array always operates close to its maximum power point, converting almost all available irradiance into DC power at the electrolyser terminals. For most irradiance and temperature conditions, the removal of the MPPT and buck converter causes the PV operating point to drift away from the true maximum power point, resulting in an effective ≈ 20% reduction in average DC power delivered. Under otherwise identical electrolyser conditions, this directly manifests as a ≈20% reduction in current density and, consequently, hydrogen production rate; stack efficiency, reversible voltage, over voltages, and hydrogen purity remain primarily controlled by pressure, temperature, and electrolyte properties rather than the power-conditioning stage.

## *V. Comparative analysis*

The solar-powered AEM electrolyser runs extremely close to its ideal current point throughout the primary daylight period when the MPPT and buck converter are active. As a result, the hydrogen production rate rapidly increases after dawn and then stays almost level and constant until sunset. The effective conversion of the available solar energy into chemical energy in the storage tank without sudden transients is indicated by the cumulative hydrogen curve, which rises steadily over this period before saturating in the evening. The created hydrogen is compressed and stored in a regulated way, as seen by the accompanying tank-pressure profile, which rises steadily and nearly linearly from the beginning value to the desired pressure before remaining constant. All things considered, MPPT greatly enhances incident irradiance utilisation and facilitates high-efficiency electrolyser operation in line with pressurised alkaline systems documented in the literature.

## *VI. Conclusion*

Overall, the simulations show that in order to extract maximum and nearly constant power from the PV array and, consequently, to operate the AEM/alkaline electrolyser close to its optimal current density over the entire effective solar window, it is essential to integrate an MPPT algorithm with a DC–DC buck converter. The cumulative hydrogen and tank pressure curves climb smoothly with MPPT, the hydrogen generation rate exhibits a broad, stable plateau, and the system behaviour closely resembles the high-efficiency pressurised alkaline electrolyser features documented in the literature. On the other hand, even while cell electrochemistry, pressure, and temperature stay constant, eliminating MPPT results in a discernible decrease in average stack current and daily hydrogen output under the same irradiance circumstances. This demonstrates that in solar-driven AEM electrolyser systems meant for realistic green hydrogen generation, PV-side power conditioning is just as crucial as stack design for attaining high hydrogen productivity, energy-conversion efficiency, and stable operation.

## *VII. References*

[1] Y. M. Berkmen and A. Lande, "Chest roentgenography as a window to the diagnosis of Takayasu's arteritis," *Am J Roentgenol Radium Ther Nucl Med*, vol. 125, no. 4, pp. 842–846, Dec. 1975, doi: 10.2214/ajr.125.4.842.

[2] A. Ursua, L. M. Gandia, and P. Sanchis, "Hydrogen Production From Water Electrolysis: Current Status and Future Trends," *Proc. IEEE*, vol. 100, no. 2, pp. 410–426, Feb. 2012, doi: 10.1109/JPROC.2011.2156750.

[3] A. Buttler and H. Spliethoff, "Current status of water electrolysis for energy storage, grid balancing and sector coupling via power-to-gas and power-to-liquids: A review," *Renewable and Sustainable Energy Reviews*, vol. 82, pp. 2440–2454, Feb. 2018, doi: 10.1016/j.rser.2017.09.003.

[4] K. Zeng and D. Zhang, "Recent progress in alkaline water electrolysis for hydrogen production and applications," *Progress in Energy and Combustion Science*, vol. 36, no. 3, pp. 307–326, Jun. 2010, doi: 10.1016/j.pecs.2009.11.002.

[5] J. Brauns and T. Turek, "Alkaline Water Electrolysis Powered by Renewable Energy: A Review," *Processes*, vol. 8, no. 2, p. 248, Feb. 2020, doi: 10.3390/pr8020248.

[6] S. Zhou, H. Ma, D. Liu, Y. Yan, S. Li, and C. Zhou, "Experimental study of a hydrogen-air rotating detonation combustor," *International Journal of Hydrogen Energy*, vol. 42, no. 21, pp. 14741–14749, May 2017, doi: 10.1016/j.ijhydene.2017.04.214.

[7] I. Vincent and D. Bessarabov, "Low cost hydrogen production by anion exchange membrane electrolysis: A review," *Renewable and Sustainable Energy Reviews*, vol. 81, pp. 1690–1704, Jan. 2018, doi: 10.1016/j.rser.2017.05.258.

[8] H. J. Burbano, J. Pareja, and A. A. Amell, "Laminar burning velocities and flame stability analysis of H2/CO/air mixtures with dilution of N2 and CO2," *International Journal of Hydrogen Energy*, vol. 36, no. 4, pp. 3232–3242, Feb. 2011, doi: 10.1016/j.ijhydene.2010.11.089.

[9] F. Barbir, "PEM electrolysis for production of hydrogen from renewable energy sources," *Solar Energy*, vol. 78, no. 5, pp. 661–669, May 2005, doi: 10.1016/j.solener.2004.09.003.

[10] A. Algarni, "Comparison of H2, CH4 and H2O for cooling an aerospace plane," *International Journal of Hydrogen*

*Energy*, vol. 21, no. 3, pp. 229–237, Mar. 1996, doi: 10.1016/0360-3199(95)00059-3.
[11] D. B. Levin, C. R. Carere, N. Cicek, and R. Sparling, "Challenges for biohydrogen production via direct lignocellulose fermentation," *International Journal of Hydrogen Energy*, vol. 34, no. 17, pp. 7390–7403, Sep. 2009, doi: 10.1016/j.ijhydene.2009.05.091.
[12] J. L. Olmedo-Martínez, B. I. Farías-Mancilla, A. Vega-Rios, and E. A. Zaragoza-Contreras, "Poly(ortho-phenylenediamine-co-aniline) based copolymer with improved capacitance," *Journal of Power Sources*, vol. 366, pp. 233–240, Oct. 2017, doi: 10.1016/j.jpowsour.2017.09.030.
[13] M. Carmo, D. L. Fritz, J. Mergel, and D. Stolten, "A comprehensive review on PEM water electrolysis," *International Journal of Hydrogen Energy*, vol. 38, no. 12, pp. 4901–4934, Apr. 2013, doi: 10.1016/j.ijhydene.2013.01.151.
[14] J. R. Varcoe *et al.*, "Anion-exchange membranes in electrochemical energy systems," *Energy Environ. Sci.*, vol. 7, no. 10, pp. 3135–3191, 2014, doi: 10.1039/C4EE01303D.
[15] H. A. Miller *et al.*, "Green hydrogen from anion exchange membrane water electrolysis: a review of recent developments in critical materials and operating conditions," *Sustainable Energy Fuels*, vol. 4, no. 5, pp. 2114–2133, 2020, doi: 10.1039/C9SE01240K.
[16] D. Pletcher and X. Li, "Prospects for alkaline zero gap water electrolysers for hydrogen production," *International Journal of Hydrogen Energy*, vol. 36, no. 23, pp. 15089–15104, Nov. 2011, doi: 10.1016/j.ijhydene.2011.08.080.
[17] D. Pletcher and X. Li, "Prospects for alkaline zero gap water electrolysers for hydrogen production," *International Journal of Hydrogen Energy*, vol. 36, no. 23, pp. 15089–15104, Nov. 2011, doi: 10.1016/j.ijhydene.2011.08.080.
[18] D. B. Levin, C. R. Carere, N. Cicek, and R. Sparling, "Challenges for biohydrogen production via direct lignocellulose fermentation," *International Journal of Hydrogen Energy*, vol. 34, no. 17, pp. 7390–7403, Sep. 2009, doi: 10.1016/j.ijhydene.2009.05.091.
[19] M. F. Ahmad Kamaroddin *et al.*, "Membrane-Based Electrolysis for Hydrogen Production: A Review," *Membranes*, vol. 11, no. 11, p. 810, Oct. 2021, doi: 10.3390/membranes11110810.
[20] H. Li, J. Guo, Z. Li, and J. Wang, "Research Progress of Hydrogen Production Technology and Related Catalysts by Electrolysis of Water," *Molecules*, vol. 28, no. 13, p. 5010, Jun. 2023, doi: 10.3390/molecules28135010.
[21] A. Abudureyimu, A. Tuluhong, Q. Chang, F. Wang, and B. Luo, "A Comprehensive Review of Green Hydrogen Technology: Electrolysis Methods, Topologies and Control Strategies, Applications," *Materials*, vol. 18, no. 21, p. 4826, Oct. 2025, doi: 10.3390/ma18214826.
[22] R. Louli, S. Giurgea, I. Salhi, S. Laghrouche, and A. Djerdir, "A Critical Review of Green Hydrogen Production by Electrolysis: From Technology and Modeling to Performance and Cost," *Energies*, vol. 19, no. 1, p. 59, Dec. 2025, doi: 10.3390/en19010059.
[23] S. A. M. Ahmed, P. Nagababu, and S. Rayalu, "Advancements in solar-powered hydrogen production: a review of concentrated solar power electrolysis, photoelectrochemical, and PV-based electrolysis," *Discov. Electrochem.*, vol. 2, no. 1, p. 68, Dec. 2025, doi: 10.1007/s44373-025-00080-4.
[24] S. Shiva Kumar and V. Himabindu, "Hydrogen production by PEM water electrolysis – A review," *Materials Science for Energy Technologies*, vol. 2, no. 3, pp. 442–454, Dec. 2019, doi: 10.1016/j.mset.2019.03.002.
[25] J. A. Carta, S. Velázquez, and J. M. Matías, "Use of Bayesian networks classifiers for long-term mean wind turbine energy output estimation at a potential wind energy conversion site," *Energy Conversion and Management*, vol. 52, no. 2, pp. 1137–1149, Feb. 2011, doi: 10.1016/j.enconman.2010.09.008.
[26] J. A. Gow and C. D. Manning, "Development of a photovoltaic arraymodel for use in power-electronics simulation studies," *IEE Proc., Electr. Power Appl.*, vol. 146, no. 2, pp. 193–200, Mar. 1999, doi: 10.1049/ip-epa:19990116.
[27] N. Femia, G. Petrone, G. Spagnuolo, and M. Vitelli, "Optimization of Perturb and Observe Maximum Power Point Tracking Method," *IEEE Trans. Power Electron.*, vol. 20, no. 4, pp. 963–973, Jul. 2005, doi: 10.1109/TPEL.2005.850975.
[28] T. Esram and P. L. Chapman, "Comparison of Photovoltaic Array Maximum Power Point Tracking Techniques," *IEEE Trans. On Energy Conversion*, vol. 22, no. 2, pp. 439–449, Jun. 2007, doi: 10.1109/TEC.2006.874230.
[29] M. A. Elgendy, B. Zahawi, and D. J. Atkinson, "Assessment of the Incremental Conductance Maximum Power Point Tracking Algorithm," *IEEE Trans. Sustain. Energy*, vol. 4, no. 1, pp. 108–117, Jan. 2013, doi: 10.1109/TSTE.2012.2202698.
[30] R. W. Erickson and D. Maksimović, *Fundamentals of Power Electronics*. Boston, MA: Springer US, 2001. doi: 10.1007/b100747.
[31] A. Pandey, N. Dasgupta, and A. K. Mukerjee, "High-Performance Algorithms for Drift Avoidance and Fast Tracking in Solar MPPT System," *IEEE Trans. Energy Convers.*, vol. 23, no. 2, pp. 681–689, Jun. 2008, doi: 10.1109/TEC.2007.914201.
[32] B. Torres, M. J. Martínez-Lope, J. A. Alonso, D. Serafini, M. T. Fernández-Díaz, and R. Martínez-Coronado, "Short communication: High-pressure synthesis and crystal structure of a novel Mg3CuHx ternary hydride," *International Journal of Hydrogen Energy*, vol. 38, no. 35, pp. 15264–15268, Nov. 2013, doi: 10.1016/j.ijhydene.2013.09.026.
[33] V. V. Golub, A. E. Korobov, A. Yu. Mikushkin, O. I. Solntsev, and V. V. Volodin, "Acceleration of hydrogen/air flames in a cylindrical envelope," *International Journal of Hydrogen Energy*, vol. 42, no. 17, pp. 12724–12734, Apr. 2017, doi: 10.1016/j.ijhydene.2017.03.177.
[34] A. Colmenar-Santos, S. Campíñez-Romero, C. Pérez-Molina, and F. Mur-Pérez, "Repowering: An actual possibility for wind energy in Spain in a new scenario without feed-in-tariffs," *Renewable and Sustainable Energy Reviews*, vol. 41, pp. 319–337, Jan. 2015, doi: 10.1016/j.rser.2014.08.041.
[35] X. He, H. Liu, S. He, B. Hu, and G. Xiao, "Research on the energy efficiency of energy regeneration systems for a battery-powered hydrostatic vehicle," *Energy*, vol. 178, pp. 400–418, Jul. 2019, doi: 10.1016/j.energy.2019.04.092.
[36] S. Kurko *et al.*, "Hydrogen sorption properties of MgH2/NaBH4 composites," *International Journal of Hydrogen Energy*, vol. 38, no. 27, pp. 12140–12145, Sep. 2013, doi: 10.1016/j.ijhydene.2013.04.075.
[37] L. Yohai, M. Vázquez, and M. B. Valcarce, "Phosphate ions as corrosion inhibitors for reinforcement steel in chloride-rich environments," *Electrochimica Acta*, vol. 102, pp. 88–96, Jul. 2013, doi: 10.1016/j.electacta.2013.03.180.
[38] Y. M. Berkmen and A. Lande, "Chest roentgenography as a window to the diagnosis of Takayasu's arteritis," *Am J Roentgenol Radium Ther Nucl Med*, vol. 125, no. 4, pp. 842–846, Dec. 1975, doi: 10.2214/ajr.125.4.842.
[39] J. N. Kamau, R. Kinyua, and J. K. Gathua, "6 years of wind data for Marsabit, Kenya average over 14m/s at 100m hub height; An analysis of the wind energy potential," *Renewable Energy*, vol. 35, no. 6, pp. 1298–1302, Jun. 2010, doi: 10.1016/j.renene.2009.10.008.
[40] P. Olivier, C. Bourasseau, and Pr. B. Bouamama, "Low-temperature electrolysis system modelling: A review," *Renewable and Sustainable Energy Reviews*, vol. 78, pp. 280–300, Oct. 2017, doi: 10.1016/j.rser.2017.03.099.
[41] M. Hammoudi, C. Henao, K. Agbossou, Y. Dubé, and M. L. Doumbia, "New multi-physics approach for modelling and design of alkaline electrolyzers," *International Journal of Hydrogen Energy*, vol. 37, no. 19, pp. 13895–13913, Oct. 2012, doi: 10.1016/j.ijhydene.2012.07.015.
[42] R. L. LeRoy, C. T. Bowen, and D. J. LeRoy, "The Thermodynamics of Aqueous Water Electrolysis," *J. Electrochem.*

*Soc.*, vol. 127, no. 9, pp. 1954–1962, Sep. 1980, doi: 10.1149/1.2130044.
[43] J. B. Share, "Review of drug treatment for Down's syndrome persons," *Am J Ment Defic*, vol. 80, no. 4, pp. 388–393, Jan. 1976.
[44] R. Gilliam, J. Graydon, D. Kirk, and S. Thorpe, "A review of specific conductivities of potassium hydroxide solutions for various concentrations and temperatures," *International Journal of Hydrogen Energy*, vol. 32, no. 3, pp. 359–364, Mar. 2007, doi: 10.1016/j.ijhydene.2006.10.062.
[45] M. P. M. G. Weijs, L. J. J. Janssen, and G. J. Visser, "Ohmic resistance of solution in a vertical gas-evolving cell," *Journal of Applied Electrochemistry*, vol. 27, no. 4, pp. 371–378, Apr. 1997, doi: 10.1023/A:1018449301423.